analytical chemistry

pubs.acs.org/ac Article

Electrochemiluminescence Sensor with Controlled-Release Triggering Electrostatic Attraction Elimination Mechanism for Trenbolone Trace Detection

Lu Zhao, Xiang Ren, Hongmin Ma, Huan Wang, Yuyang Li, Qin Wei, Dan Wu,* and Huangxian Ju

Cite This: *Anal. Chem.* 2023, 95, 13463−13469 Read Online

ACCESS | Metrics & More | Article Recommendations | Supporting Information

ABSTRACT: A controlled-release strategy can meet the needs of sensitive environmental monitoring for pollutants through a self-on/off mode. In this work, an electrochemiluminescence (ECL) biosensor with controlled-release triggering electrostatic attraction elimination and biomolecular stimulated response strategies was constructed to detect environmental steroid hormones sensitively. The blocked pores on the aminated mesoporous silica nanocontainers were opened by specific binding between the trenbolone (TB) antigen and the antibody. The released L-cysteine counteracted the negative charge on the MnO_2 NF surface through the redox reaction between −SH and MnO_2, making the electrostatic interaction between the MnO_2 NFs and the $Ru(dcbpy)_3^{2+}$ disappear. $Ru(dcbpy)_3^{2+}$ released an ECL signal on the electrode, thus completing the controlled-release triggering electrostatic attraction elimination strategy. In addition, with the TB antibody as the target and the competition strategy between the TB antigen and the standard substance, the constructed controlled-release ECL biosensor was used to detect the TB standard substance. Moreover, MnO_2 NFs as the substrate of the ECL biosensor increased the active specific surface area of the electrode, effectively catalyzing the production of $OH^•$ and $O_2^{•-}$, thus endowing the ECL biosensor with coreactant-catalytic enhancement characteristic and further improving its ECL performance. This sensitive signal response brought about a low limit of detection of 2.53 fg/mL for the constructed ECL biosensor, which contributed a feasible idea for efficient trace analysis of pollutants in the environment.

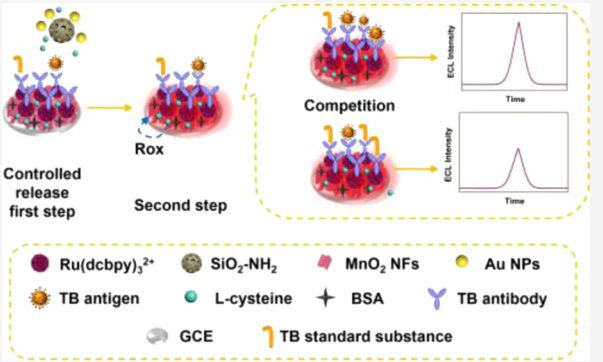

INTRODUCTION

Steroid hormones, which are referred to a kind of exogenous compounds similar to estrogen activity in organisms, are widely known to disorganize the endocrine system of humans.[1,2] Trenbolone (TB) is a steroid hormone that can interfere with the endocrine activity of organisms and is classified as a kind of emerging contaminant (EC). It is used by more and more athletes and fitness enthusiasts to strengthen their muscles and increase their dimension and strength, as well as in some cosmetics.[3−5] TB will affect the genital system of the human body, thus inducing breast, testicular, and uterine cancers and other diseases, and will also lead to the birth of deformed children. In addition, if the urine, sweat, or industrial wastewater containing TB is discharged into the natural environment or even used for aquaculture, the male and female ratio of fish and other animals will be imbalanced and ecological production will be endangered.[1−4,6] Therefore, the efficient and sensitive analysis of trace TB in environmental water is crucial for the treatment of the ecological environment.

In terms of the detection of TB, most of the methods reported in the literature are liquid chromatography-tandem mass spectrometry[7] and collisionally activated dissociation mass-analyzed ion kinetic energy spectrometry.[8] Compared with them, the electrochemiluminescence (ECL) immunoassay technique has characteristics of low background, plain operation, wide dynamic ranges, high sensitivity, and stability. Therefore, the ECL immunoassay technique can meet the requirements of trace and transient response in environmental monitoring.[9,10] Even, the biosensor constructed with ECL technology can also realize the clinical detection of urine and sweat to determine whether the patient has excessive absorption of TB. It is worth mentioning that the introduction of a controlled-release strategy can make the ECL biosensor possess self-on or self-off mode by stimuli response like pH, biomolecule, and light. The controllable characteristic can make the work of the ECL sensor more accurate and reflect the detected object more strongly and sensitively.[9,11−14]

Received: March 29, 2023
Accepted: August 17, 2023
Published: August 30, 2023

https://doi.org/10.1021/acs.analchem.3c01359
Anal. Chem. 2023, 95, 13463−13469

Scheme 1. Synthesis Route of the SiO_2−NH_2/Au NPs−TB Antigen, the Fabrication Process, and Related Mechanisms of the Constructed Controlled-Release ECL Biosensor

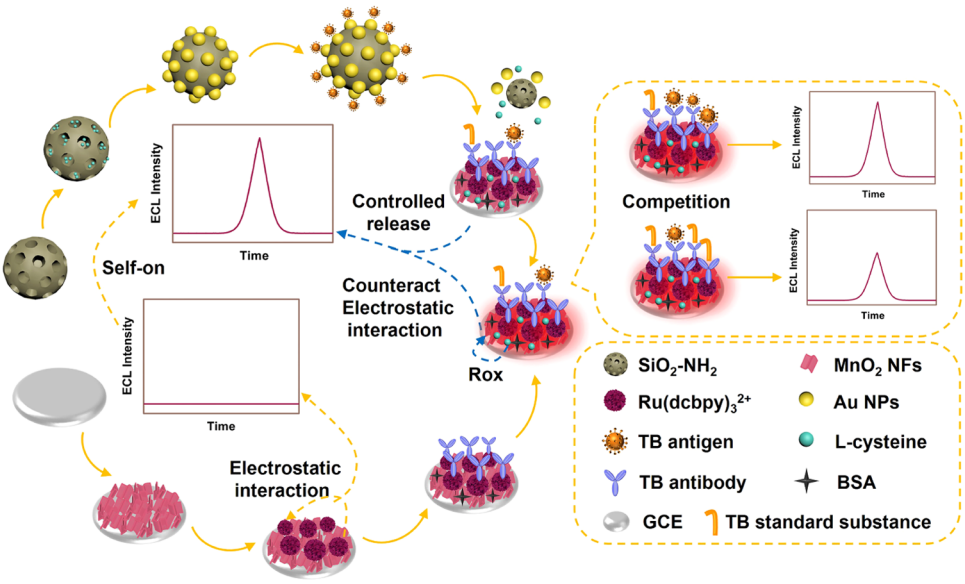

Nowadays, there have been few reports in regard to the controlled release of ECL biosensors. The reported controlled-release ECL biosensors were used for the detection of aminotriazole and Hg^{2+}.[9,11] In this work, we have constructed a controlled-release ECL system using aminated mesoporous silica nanocontainers (SiO_2−NH_2) as a carrier and Ru(dcbpy)$_3^{2+}$ as a luminophore. SiO_2−NH_2 is an ideal material for the controlled-release carrier with merits of good biocompatibility, biodegradability, and uniform and tunable pore size.[15,16] Au NPs matching the pore size of SiO_2−NH_2 were used as blocking agents through Au−NH_2 bonding. Subsequently, Au NPs were connected with the TB antigen via Au−NH_2 bonding,[17] forming the controlled-release biological complex. After the TB antibody stimulated response, the TB antigen competed with the standard substance, releasing L-cysteine (L-Cys) from SiO_2−NH_2 to eliminate the negative charge on the surface of MnO_2 NFs via its sulfhydryl group.[18] Based on this strategy, the electrostatic interaction between MnO_2 NFs and Ru(dcbpy)$_3^{2+}$ disappeared. Therefore, Ru(dcbpy)$_3^{2+}$ released an ECL signal on the electrode, realizing the self-on mode of the constructed controlled-release ECL biosensor.[18] In addition, the as-synthesized MnO_2 NFs had a large specific surface area and more active sites, which can load more Ru(dcbpy)$_3^{2+}$ and catalyze the generation of coreactant radicals efficiently, endowing the controlled-release ECL biosensor with coreactant-catalytic enhancement performance. Thus, the constructed controlled-release ECL biosensor exhibited good accuracy and sensitivity with a low limit of detection of 2.53 fg/mL, which can realize the trace analysis for TB.

EXPERIMENTAL SECTION

Synthesis of MnO_2 NFs. A 0.002 mol amount of 2-morpholinoethanesulfonic acid and 0.2 mmol $KMnO_4$ were dispersed in 20 mL of H_2O under ultrasonication and stirred for 30 min. The blank powders were centrifuged and washed with H_2O three times, dried at 60 °C, and then harvested.

Synthesis of SiO_2−NH_2. Overall, 0.5 g of cetyltrimethylammonium bromide was dissolved in 200 mL of ultrapure water, and then 1.75 mL of a 2.0 M NaOH solution was added to the cetyltrimethylammonium bromide solution and stirred for 20 min at 80 °C. Then, 2.5 mL of tetraethyl orthosilicate was added to the mixture and stirred for 2 h until the white precipitates appeared. The obtained precipitates were centrifuged and washed with ultrapure water 2 times and methanol 1 time orderly to obtain the SiO_2 powders. Next, the SiO_2 powders were dissolved in a mixture of 1.5 mL of HCl and 75 mL of methanol. The reaction went through reflux for 10 h, and the products were centrifuged and washed 6 times alternately with ultrapure water and methanol. Then, 240 mg of the dried products was reacted with 240 μL of (3-aminopropyl) triethoxysilane (APTES) in 12 mL of anhydrous ethanol, and then refluxed for 12 h at 80 °C. SiO_2−NH_2 was obtained after centrifuging 3 times with ultrapure water and vacuum drying at 60 °C.

Synthesis of the Au NPs−TB Antigen Bioconjugate. Au NPs were prepared by citrate reduction of $HAuCl_4$·$4H_2O$ based on a classic method with certain modifications.[19] First, 1 mL of 1% $HAuCl_4$ was diluted in 100 mL of ultrapure water. Next, 2.5 mL of 1% $C_6H_5Na_3O_7$·$2H_2O$ was added under vigorous stirring and boiled for 10 min. After stirring for another 10 min, the solution was cooled to room temperature and stored at 4 °C. Then, the Au NP solution was adjusted to pH 9 via a Na_2CO_3 solution. Then, 200 μL of a 1 μg/mL TB antigen was added into 10 mL of the adjusted Au NP solution, and the evenly shaken mixture was incubated at 4 °C for 12 h. Subsequently, the mixture was centrifuged at 4 °C for 30 min and washed twice with a PBS solution (pH = 7.4). Finally, the product was dissolved in 1 mL of a PBS solution (1.0 wt % BSA) and stored at 4 °C to obtain the Au NPs−TB antigen bioconjugate.

Encapsulation of L-Cys and the Synthesis of SiO_2−NH_2/Au NPs−TB Antigen. One milliliters of a 10 mg/mL L-Cys solution was added to 1 mL of a SiO_2−NH_2 solution (10 mg/mL) and shaken for 12 h. The mixture was centrifuged for 5 min and washed 3 times with a PBS solution (pH = 7.4). Then, 100 μL of a Au NPs−TB antigen bioconjugate solution was injected into the mixture and incubated at 4 °C for 12 h.

https://doi.org/10.1021/acs.analchem.3c01359
Anal. Chem. 2023, 95, 13463−13469

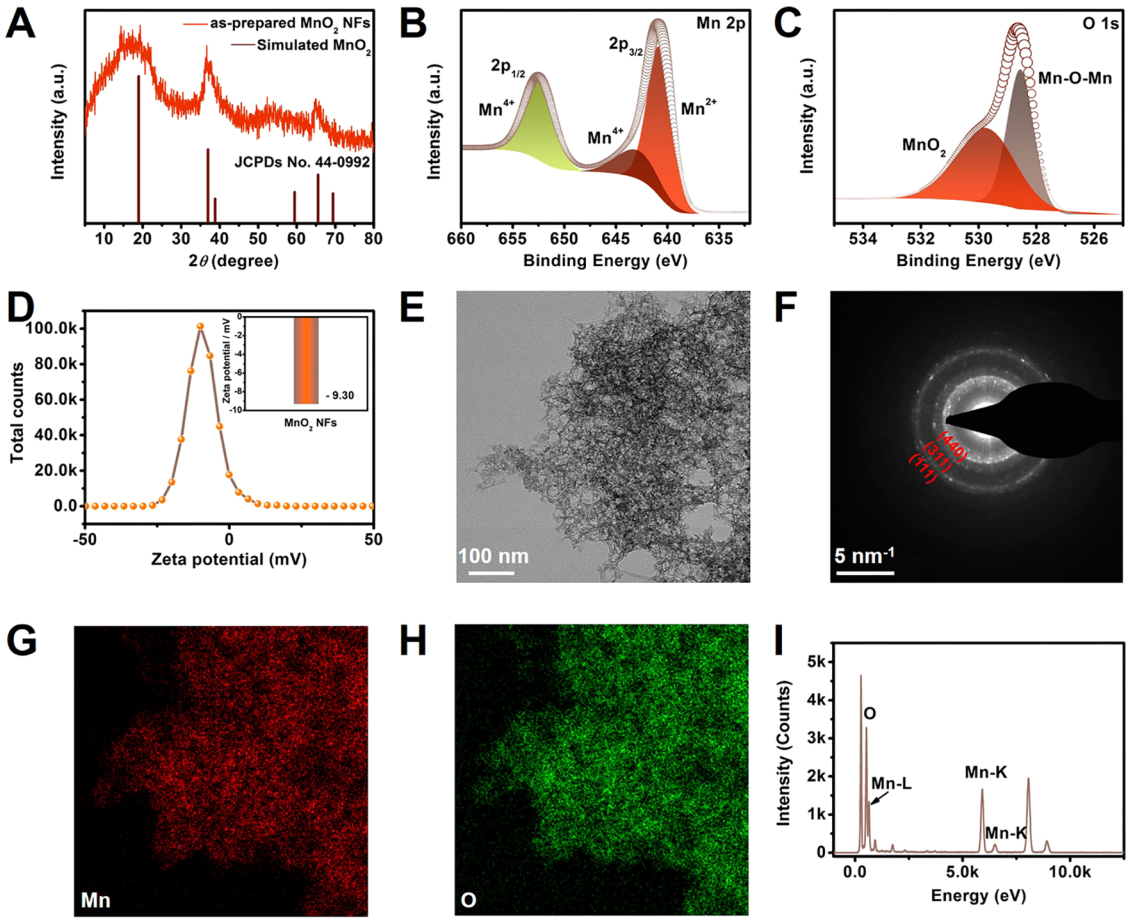

Figure 1. (A) XRD patterns of simulated and as-synthesized MnO_2 NFs. XPS spectra in the (B) Mn 2p and (C) O 1s regions. (D) ζ potential, (E) TEM image, (F) SAED pattern, (G, H) elemental mapping, and (I) EDS spectrum of the as-synthesized MnO_2 NFs.

After centrifuging and washing 3 times with a PBS solution (pH 7.4), the obtained SiO_2−NH_2/Au NPs−TB antigen complex was dissolved in 1 mL of a PBS solution and stored at 4 °C.

Fabrication Process of the ECL Biosensor. The fabrication of the sensing interface is shown in Scheme 1. After the glassy carbon electrode (GCE) was polished, 8 μL of a 6 mg/mL MnO_2 NF solution, 8 μL of an 8 mg/mL $Ru(dcbpy)_3^{2+}$ solution, 6 μL of a 1 μg/mL TB antibody, 3 μL of a 1% BSA solution, 6 μL of a TB standard substance, and a SiO_2−NH_2/Au NPs−TB antigen mixture were modified onto the GCE surface orderly. After each step was accomplished, the GCE was washed with water and then stored at 4 °C.

ECL Measurement of the TB Standard Substance. The performance of the constructed two-step controlled-release ECL biosensor was examined under the scanning range of 0.5−1.2 V in 15 mL of phosphate-buffered saline (PBS) (pH = 7.4) at a photomultiplier tube voltage of 700 V.

RESULTS AND DISCUSSION

Characterizations of MnO_2 NFs. The X-ray diffraction patterns (XRD) and X-ray photoemission spectroscopy were used to verify the successful synthesis of MnO_2 NFs from their crystal phase information, structural composition, and element valence. From Figure 2A, three obvious peaks at 19.1, 37.1, and 65.7° were attributable to the crystallographic planes of (111), (311), and (440), respectively, which are assigned to MnO_2 (JCPDs no. 44-0992). The complete chemical compositions of MnO_2 NFs were revealed by X-ray photoelectron spectroscopy (XPS) survey spectrum in Figure S1. Specifically, in the high-resolution Mn 2p spectrum (Figure 1B), the $2p_{3/2}$ energy level was divided into two peaks at 640.8 and 642.8 eV, which corresponded to Mn^{2+} and Mn^{4+}.[20] The difference between binding energies of $2p_{3/2}$ (642.8 eV) and $2p_{1/2}$ (652.5 eV) conformed to the literature report, indicating the Mn^{4+} peak of $2p_{1/2}$ in MnO_2.[20,21] In the O 1s spectrum (Figure 1C), the high peaks at 528.5 and 529.7 eV were attributed to Mn−O−Mn and MnO_2, respectively, which confirmed the successful synthesis of MnO_2 NFs.[22] In Figure 1D, ζ potential results showed that the MnO_2 NF surface carried the average charge of −9.30 mV. As the substrate of the biosensor, the negative charge carried by the MnO_2 NFs themselves can attract the $[Ru(dcbpy)_3]^{2+}$ via electrostatic interaction, thus blocking the ECL signal generation.[18] In addition, the MnO_2 NFs possessed nanoflake morphology with a thickness of several nanometers (Figure 1E). A detailed analysis of the selected area electron diffraction (SAED) pattern of MnO_2 NFs (Figure 1F) exhibited a cubic structure with distinct rings consistent with the (440), (311), and (111) planes. The observed elements of Mn and O contained in MnO_2 NFs were evenly distributed (Figure 1G,H). In Figure 1I, energy dispersive spectroscopy (EDS) of the O, Mn L, and Mn K maps was presented. To summarize, MnO_2 NFs with a negative charge on the surface were successfully synthesized.

Characterizations of SiO_2−NH_2 and SiO_2−NH_2/Au NPs−TB Antigen. First, the successful synthesis of SiO_2−

https://doi.org/10.1021/acs.analchem.3c01359
Anal. Chem. 2023, 95, 13463−13469

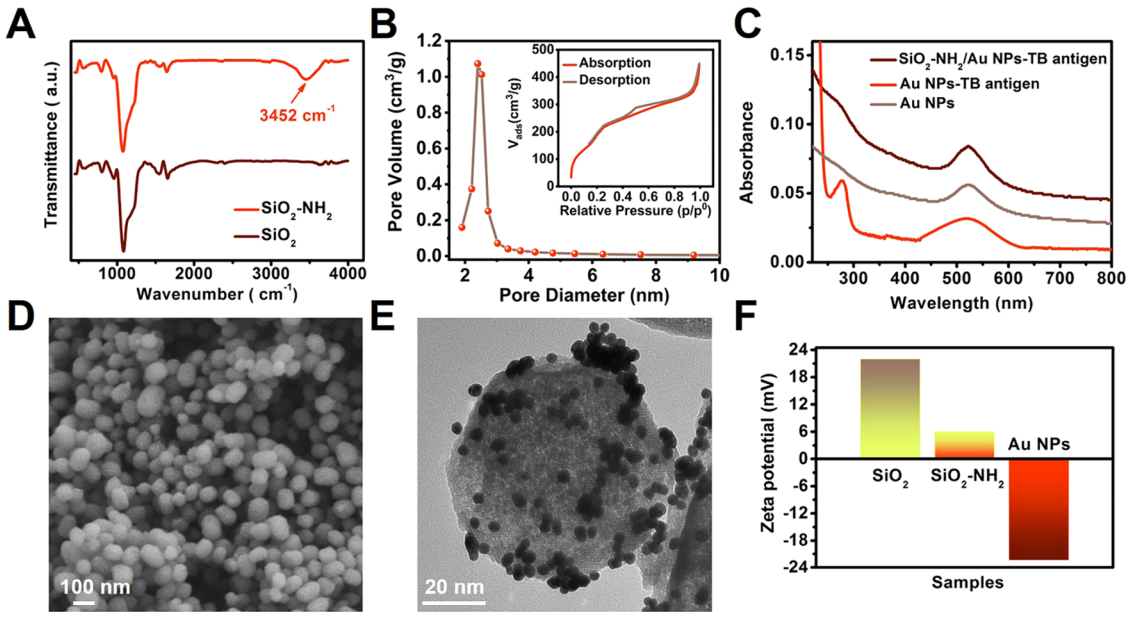

Figure 2. (A) FTIR spectra of as-synthesized SiO_2 and SiO_2−NH_2. (B) Pore-size distribution of SiO_2−NH_2; the inset figure shows the nitrogen adsorption−desorption isotherm of SiO_2−NH_2. (C) UV−vis spectra of Au NPs, Au NPs−TB antigen, and SiO_2−NH_2/Au NPs−TB antigen. (D) SEM image of SiO_2−NH_2. (E) TEM image of SiO_2−NH_2/Au NP−TB antigen. (F) ζ potentials of SiO_2, SiO_2−NH_2, and Au NPs.

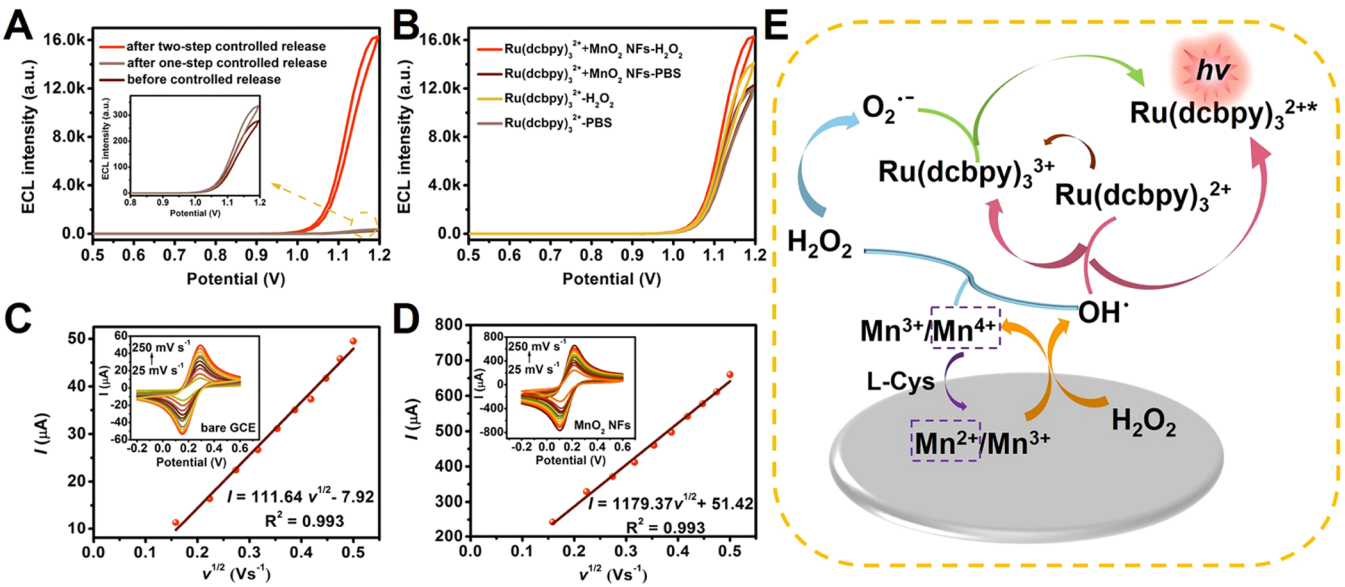

Figure 3. (A) ECL−potential curves of the constructed ECL biosensor before the controlled-release process (curve brown), after only the controlled-release process (curve gray), and after the electrostatic attraction elimination process (curve orange). (B) ECL−potential curves of different systems: bare $Ru(dcbpy)_3^{2+}$ in bare PBS and PBS-contained H_2O_2 and $Ru(dcbpy)_3^{2+}$−MnO_2 NFs in bare PBS and PBS-contained H_2O_2. (C, D) CV curves and linear equations of bare GCE and the electrode modified with MnO_2 NFs in 5.0 mmol/L $[Fe(CN)_6]^{3-/4-}$ in the scan rate range of 25−250 mV/s. (E) Conjectural mechanism of the constructed controlled-release ECL biosensor.

NH_2 was verified through FTIR spectra. The FTIR spectrum of SiO_2−NH_2 was almost the same as that of pure SiO_2, except that SiO_2−NH_2 has an extra characteristic peak of the stretching vibration for −NH at 3452 cm^{-1} (Figure 2A), indicating the successful synthesis of SiO_2−NH_2.[23] The mesoporous property of the as-synthesized SiO_2−NH_2 was confirmed according to a type-IV isotherm embodied from the N_2 adsorption−desorption isotherm (Figure 2B).[15] In the Brunauer−Emmet−Teller (BET) test results, the surface area was 860.85 m^2/g, and the pore volume was 0.768 cm^3/g with a narrow BJH pore-size distribution of the average pore diameter of 2.43 nm (Figure 2B). Next, the successful synthesis of the SiO_2−NH_2/Au NPs−TB antigen was verified through UV−vis spectra. In Figure 2C, the absorption peaks at 272 and 518 nm both correspond to the characteristic bands of the antigen and Au NPs. The blue shift in the characteristic bands of the antigen and the narrowing for the characteristic bands of Au NPs occurred in SiO_2−NH_2/Au NPs−TB antigen, which displayed the successful connection between the SiO_2−NH_2 and Au NPs−TB antigen bioconjugate.[24] The morphology of SiO_2−NH_2 was presented as a spherical shape with an average diameter of 70 nm (Figure 2D). After the electrostatic

https://doi.org/10.1021/acs.analchem.3c01359
Anal. Chem. 2023, 95, 13463−13469

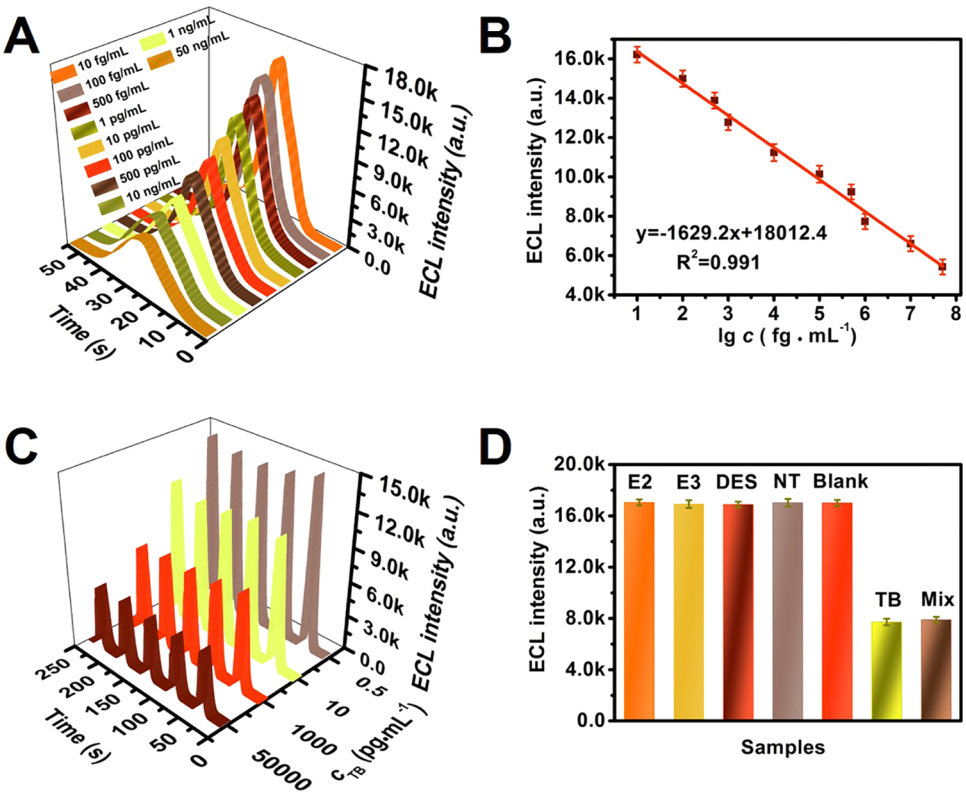

Figure 4. (A) ECL intensity−time curves and (B) linear relation of the proposed ECL biosensor for TB detection under a concentration gradient (10 fg/mL to 50 ng/mL). (C) Stability of the constructed ECL biosensor determined under different concentrations of TB. (D) Selectivity tests of the proposed ECL biosensor for different interferences. Error bars = SD, (n = 3).

adsorption of Au NPs, the SiO_2−NH_2 nanospheres were encircled uniformly by Au NPs with a 5 nm diameter (Figure 2E). In the results of ζ potential (Figure 2F), SiO_2 and SiO_2−NH_2 carried positive charges, and the Au NPs carried negative charges,[25] proving the possibility of electrostatic adsorption between Au NPs and SiO_2−NH_2.

Controlled Release Triggering Electrostatic Attraction Elimination Strategy of the Constructed ECL Biosensor. For the controlled-release triggering electrostatic attraction elimination strategy, the schematic diagram is shown in Scheme 1 and Figure 3A. First, compared with the Au−NH_2 bonding, the specific binding between the TB antigen and the antibody was stronger. Therefore, the TB antigen−Au NPs bioconjugate fell off the surface of SiO_2−NH_2, thereby opening the blocked pores and releasing L-Cys (controlled-release process). Second, the released L-Cys counteracts the negative charge on the surface of MnO_2 NFs through the oxidation−reduction reaction between −SH and MnO_2, thus eliminating the electrostatic attraction effect between MnO_2 and Ru(dcbpy)$_3^{2+}$ (electrostatic attraction elimination process). Finally, Ru(dcbpy)$_3^{2+}$ was released to the surface of the electrode, realizing the "off-on" ECL signal mode.

Speculation of the ECL Enhanced Mechanism. The production of coreactant radicals $OH^•$ and $O_2^{•-}$ through the catalysis of MnO_2 NFs is one of the mechanisms that make the constructed ECL biosensor have a coreactant-catalytic enhancement function. The electron paramagnetic resonance experiment with DMPO as a radical scavenger was used to explore the production of radicals $OH^•$ and $O_2^{•-}$ after the catalysis of MnO_2 NFs. As shown in Figure S2, obvious radical peaks of $OH^•$ and $O_2^{•-}$ were observed under the catalysis of MnO_2 NFs, and the weak peaks were observed under the situation of no catalyst. Therefore, in the ECL process, the reaction of Mn^{2+} and H_2O_2 generated $OH^•$ at the same time as Mn^{4+}, and subsequently, Mn^{4+} reacted with H_2O_2 and $OH^•$ to make $O_2^{•-}$. $OH^•$ reacted with Ru(dcbpy)$_3^{2+}$ and $O_2^{•-}$ reacted with Ru(dcbpy)$_3^{3+}$, generating Ru(dcbpy)$_3^{2+*}$ to produce ECL. The whole conjectural ECL mechanisms are displayed in the form of equations and Figure 3E, as follows[18,26−30]

Path 1

$$Mn^{2+} + H_2O_2 \rightarrow Mn^{3+} + OH^• + OH^- \quad (1)$$

$$Mn^{3+} + H_2O_2 \rightarrow Mn^{4+} + OH^• + OH^- \quad (2)$$

$$Mn^{4+} + H_2O_2 + OH^• \rightarrow Mn^{4+} + O_2^{•-} + H_2O + H^+ \quad (3)$$

$$Mn^{4+} + L - Cys \rightarrow Mn^{2+} + products \quad (4)$$

Path 2

$$Ru(dcbpy)_3^{2+} - e^- \rightarrow Ru(dcbpy)_3^{3+} \quad (5)$$

$$Ru(dcbpy)_3^{2+} + OH^• \rightarrow Ru(dcbpy)_3^{3+} + OH^- \quad (6)$$

$$Ru(dcbpy)_3^{3+} + OH^- \rightarrow Ru(dcbpy)_3^{2+*} + products \quad (7)$$

$$Ru(dcbpy)_3^{3+} + O_2^{•-} \rightarrow Ru(dcbpy)_3^{2+*} + O_2 \quad (8)$$

$$Ru(dcbpy)_3^{2+*} \rightarrow Ru(dcbpy)_3^{2+} + h\nu \quad (9)$$

For the ECL−potential curves of bare Ru(dcbpy)$_3^{2+}$ and Ru(dcbpy)$_3^{2+}$−MnO_2 NF system in a PBS solution with H_2O_2,

https://doi.org/10.1021/acs.analchem.3c01359
Anal. Chem. 2023, 95, 13463−13469

the ECL signals were 16 300 and 14 100 au, respectively. However, the low ECL signals for bare $Ru(dcbpy)_3^{2+}$ and $Ru(dcbpy)_3^{2+}$−MnO_2 NF systems in a pure PBS solution had little difference (Figure 3B). These findings confirmed the catalysis of MnO_2 NFs for only H_2O_2 rather than $Ru(dcbpy)_3^{2+}$.

Another way for the MnO_2 NFs to enhance the ECL performance of the constructed biosensor is to effectively increase the surface area of the substrate and the load capacity of $Ru(dcbpy)_3^{2+}$. Cyclic voltammetry (CV) was tested, and the electroactive surface area of the MnO_2 NF-modified GCE and bare GCE were calculated to verify this enhancement of MnO_2 NFs. CV was conducted under a $K_3[Fe(CN)_6]$ solution, and the calculations proceeded according to the Randles−Sovcik formula[31,32]

$$I = 2.69 \times 10^5 AD^{1/2} n^{3/2} v^{1/2} c$$

in which n, I, D, v, A, and c are the number of electron transfer, the reduction current maximum of $K_3[Fe(CN)_6]$, the diffusion coefficient of $[Fe(CN)_6]^{3-/4-}$ at room temperature, the scanning rate, the calculated electrochemical active area (cm^2), and the concentration of the $K_3[Fe(CN)_6]$ solution, respectively.

By virtue of the linear equation of reduction current values and scan rates (Figure 3C,D) (MnO_2 NFs: $I = 1179.37v^{1/2} + 51.42$, $R^2 = 0.993$; bare GCE: $I = 111.64v^{1/2} - 7.92$, $R^2 = 0.993$), the obtained A value of MnO_2 NF-modified GCE is 33.88 mm^2, bigger than 3.20 mm^2 of bare GCE, illustrating the obvious magnification of the electroactive surface area for MnO_2 NFs. In addition, the acceleration of the electron transfer rate was certified via the enhancement of current responses of MnO_2 NFs compared with bare GCE. These results meant the good catalytic performance of MnO_2 NFs to realize the coreactant-catalytic enhancement of the constructed biosensor.

Performance Analysis of the Constructed Controlled-Release ECL Biosensor. The completion of the construction for the biosensor was confirmed via the CV and EIS test results (Figure S3). All of the ECL performance tests of the biosensor were conducted under optimal conditions (Figure S4). Then, we used the constructed biosensor to detect TB standard substances quantitatively through a competitive mechanism. Both the standard substance and the antigen can bind specifically to the antibody. The binding ability of the antibody for the TB standard substance is preferred to antigens due to the small molecular characteristic of the TB standard substance. Therefore, the changes in the concentration of the TB standard substance can affect the amount of released L-Cys with an inversely proportional relationship. Combined with the counteraction of L-Cys for electrostatic interaction, the amount of released L-Cys can be related to the amount of released $Ru(dcbpy)_3^{2+}$, thus influencing the ECL signals. Therefore, as shown in Figure 4A,B, the biosensor signals decreased linearly with the increase of TB standard substance concentrations, and the related linear relation was $I = -1629.2 \lg c + 18012.4$ ($R^2 = 0.991$). The estimated limit of detection (LOD) was 2.53 fg/mL, which exhibited a more sensitive performance than that of many other detection methods, as Table S1 shows, illustrating the outstanding potentiality of the suggested biosensor in environmental analysis.

In addition, stability, selectivity, and reproducibility are also important evaluation criteria for estimating the analytical performance of a biosensor. Under the optimized conditions, the ECL signals of the constructed biosensor with different TB standard substance concentrations showed a stable tendency (Figure 4C), indicating the favorable stability of the proposed biosensor. Next, the ECL signals with different interferences, including diethylstilbestrol (DES), nortestosterone (NT), estradiol (E2), and estriol (E3), were tested. As shown in Figure 4D, the strong ECL signals were exhibited for interferents (10 ng/mL) and blank sample, and the weak ECL signals were exhibited for TB standard substances (1 ng/mL) and the mixture (TB standard substances of 1 ng/mL + interferents of 10 ng/mL), which demonstrated the good selectivity for the constructed biosensor to detect TB. Finally, in Figure S5, six biosensors were constructed in the same environment to determine TB standard substances simultaneously. The fine distinction between the seven constructed biosensors with 1.5% RSD indicates the superior reproducibility of the constructed ECL biosensor.

The real sample analysis is a measurement to estimate the practicability of the proposed ECL biosensor. The initial concentrations of real water samples were obtained from three rivers and measured 3 times to acquire averages. Subsequently, the recovery rates and RSD values were calculated using the standard addition method. After the addition of TB standard substances into water samples, the calculated recovery rate ranged from 98.0 to 101%, and the calculated RSD ranged from 1.3 to 3.0% (Table S2). The good accuracy and precision of the proposed ECL biosensor can confirm a feasible approach for the trace detection of TB in the domestic water, industrial wastewater, and agricultural water absolutely.

CONCLUSIONS

To summarize, an efficient controlled-release ECL biosensor was constructed to detect trace TB in environmental water with three mechanisms. On the one hand, the controlled-release triggering electrostatic attraction elimination process realized the release of $Ru(dcbpy)_3^{2+}$ and the generation of the ECL signals. On the other hand, the competitive mechanism from the TB standard substance and the antigen to the specific binding sites of the TB antibody triggered a linear signal response to the concentration of the TB standard substance. In addition, the large specific surface area of MnO_2 NFs made them have high catalytic efficiency for H_2O_2 and promoted the formation of more $OH^{\bullet}$ and $O_2^{\bullet-}$, further increasing the ECL signals to bring up the coreactant-catalytic enhancement characteristic. Compared with traditional detection methods of TB, this ECL biosensor integrating three strategies greatly improved the sensitivity and accuracy of TB detection. In addition, after analyzing the real samples, it was verified that the construction methods of the ECL biosensor were feasible and could meet the needs of environmental monitoring in environmental protection, industry, and other industries.

ASSOCIATED CONTENT

Supporting Information

The Supporting Information is available free of charge at https://pubs.acs.org/doi/10.1021/acs.analchem.3c01359.

Chemicals and apparatus, synthesis of $[Ru(H_2dcbpy)_3]\cdot Cl_2$, XPS of MnO_2 NFs, EPR spectra under the MnO_2 NF catalyst and no catalyst, electrochemical performance of the biosensor, optimization of experimental conditions, reproducibility of the constructed ECL biosensor, comparison of different methods and

https://doi.org/10.1021/acs.analchem.3c01359
Anal. Chem. 2023, 95, 13463−13469

biosensors for TB detection, and standard addition data of the proposed ECL biosensor for real samples (PDF)

AUTHOR INFORMATION

Corresponding Author

Dan Wu − *School of Chemistry and Chemical Engineering, University of Jinan, Jinan 250022, P. R. China;* orcid.org/0000-0002-8732-5988; Phone: +86 531 82765730; Email: wudan791108@163.com; Fax: +86 531 82765969

Authors

Lu Zhao − *School of Chemistry and Chemical Engineering, University of Jinan, Jinan 250022, P. R. China*

Xiang Ren − *School of Chemistry and Chemical Engineering, University of Jinan, Jinan 250022, P. R. China;* orcid.org/0000-0002-4321-4282

Hongmin Ma − *School of Chemistry and Chemical Engineering, University of Jinan, Jinan 250022, P. R. China;* orcid.org/0000-0002-7061-8944

Huan Wang − *School of Chemistry and Chemical Engineering, University of Jinan, Jinan 250022, P. R. China;* orcid.org/0000-0002-0855-1427

Yuyang Li − *School of Chemistry and Chemical Engineering, University of Jinan, Jinan 250022, P. R. China;* orcid.org/0000-0002-1399-9381

Qin Wei − *School of Chemistry and Chemical Engineering, University of Jinan, Jinan 250022, P. R. China;* orcid.org/0000-0002-3034-8046

Huangxian Ju − *School of Chemistry and Chemical Engineering, University of Jinan, Jinan 250022, P. R. China;* orcid.org/0000-0002-6741-5302

Complete contact information is available at: https://pubs.acs.org/10.1021/acs.analchem.3c01359

Notes

The authors declare no competing financial interest.

ACKNOWLEDGMENTS

This work was supported by the National Natural Science Foundation of China (22274063) and the Young Taishan Scholars Program of Shandong Province (tsqn201909124). All of the authors express their sincere thanks.

REFERENCES

(1) Chen, X. H.; Pan, S. D.; Ye, M. J.; Li, X. P.; Zhao, Y. G.; Jin, M. C. *J. Sep. Sci.* **2016**, *39*, 762−768.

(2) Collier, A.; Wang, J.; Diamond, D.; Dempsey, E. *Anal. Chim. Acta* **2005**, *550*, 107−115.

(3) Pacáková, V.; Loukotková, L.; Bosáková, Z.; Stulík, K. *J. Sep. Sci.* **2009**, *32*, 867−882.

(4) Kolodziej, E. P.; Qu, S.; Forsgren, K. L.; Long, S. A.; Gloer, J. B.; Jones, G. D.; Schlenk, D.; Baltrusaitis, J.; Cwiertny, D. M. *Environ. Sci. Technol.* **2013**, *47*, 5031−5041.

(5) Khetan, S. K.; Collins, T. J. *Chem. Rev.* **2007**, *107*, 2319−2364.

(6) Zhao, L.; Wang, M.; Song, X. Z.; Liu, X. J.; Ju, H. X.; Ai, H. Q.; Wei, Q.; Wu, D. *Chem. Eng. J.* **2022**, *434*, No. 134691.

(7) Blackwell, B. R.; Cai, Q.; Smith, P. N.; Cobb, G. P. *Talanta.* **2011**, *85*, 1317−1323.

(8) Facino, R. M.; Carini, M.; Forno, A. D.; Traldi, P.; Pompa, G. *Biomed. Mass Spectrom.* **1986**, *13*, 121−127.

(9) Liu, G. Y.; Ling, J.; Li, J. P. *ACS Sens.* **2021**, *6*, 4185−4192.

(10) Song, X. Z.; Ren, X.; Zhao, W.; Zhao, L.; Wang, S. F.; Luo, C. N.; Li, Y. Y.; Wei, Q. *Anal. Chem.* **2022**, *94*, 12531−12537.

(11) Li, L. B.; Zhao, W. L.; Zhang, J. Y.; Luo, L. J.; Liu, X. H.; Li, X.; You, T. Y.; Zhao, C. J. *J. Colloid Interface Sci.* **2022**, *608*, 1151−1161.

(12) Thornton, P. D.; Mart, R. J.; Ulijn, R. V. *Adv. Mater.* **2007**, *19*, 1252−1256.

(13) Wang, F. T.; Huang, K. J.; Hou, Y. Y.; Tan, X. C.; Wu, X.; Yu, X. M.; Zhou, X. *Nanoscale* **2022**, *14*, 815−822.

(14) Hou, Y. Y.; Xu, J.; Xie, W. Z.; Huang, K. J.; Tan, X. C.; Zhao, B. R.; Zhang, S. Q.; Gao, M. T. *Sens. Actuators, B* **2023**, *376*, No. 132998.

(15) Ma, N.; Ren, X.; Wang, H.; Kuang, X.; Fan, D. W.; Wu, D.; Wei, Q. *Anal. Chem.* **2020**, *92*, 14069−14075.

(16) Pan, J. M.; Wu, R. R.; Dai, X. H.; Yin, Y. J.; Pan, G. Q.; Meng, M. J.; Shi, W. D.; Yan, Y. S. *Biomacromolecules* **2015**, *16*, 1131−1145.

(17) Xu, J.; Wang, Y. H.; Wei, Z. N.; Wang, F. T.; Huang, K. J. *Sens. Actuators, B* **2021**, *327*, No. 128933.

(18) Li, H. Y.; Lv, W. X.; Yang, Q. T.; Li, Q.; Li, F. *J. Agric. Food Chem.* **2021**, *69*, 6087−6095.

(19) Wang, X.; Chen, Y.; Fang, Y. J.; Zhang, J. T.; Gao, S. Y.; Lou, X. W. *Angew. Chem. Int. Ed.* **2019**, *58*, 2675−2679.

(20) Jia, H. N.; Cai, Y. F.; Zheng, X. H.; Lin, J. H.; Liang, H. Y.; Qi, J. L.; Cao, J.; Feng, J. C.; Fei, W. D. *ACS Appl. Mater. Interfaces* **2018**, *10*, 38963−38969.

(21) Wang, J. H.; Guo, X. H.; Cu, R. L.; Huang, H.; Liu, B.; Li, Y.; Wang, D.; Zhao, D. G.; Dong, J. Q.; Li, S. C.; Sun, B. Y. *ACS Appl. Nano Mater.* **2020**, *3*, 11152−11159.

(22) Dai, Y. M.; Tang, S. C.; Vongehr, S.; Meng, X. K. *ACS Sustainable Chem. Eng.* **2014**, *2*, 692−698.

(23) Liu, Y. F.; Li, B.; Tu, F. F.; Liang, C.; Gao, M. X.; Pan, H. G.; Wang, Q. D. *Dalton Trans.* **2011**, *40*, 8179−8186.

(24) Yuan, L.; Yu, J.; Wang, S.; Huang, K. K.; Ren, X. R.; Sun, Y.; Wu, X. F.; Feng, S. H. *Mater. Lett.* **2015**, *143*, 212−214.

(25) Xu, J.; Liu, Y. B.; Huang, K. J.; Hou, Y. Y.; Sun, X. X.; Li, J. Q. *Anal. Chem.* **2022**, *94*, 16980−16986.

(26) Chen, Q. B.; Ma, Y.; Bai, P.; Li, Q.; Canup, B. S. B.; Long, D. P.; Ke, B. W.; Dai, F. Y.; Xiao, B.; Li, C. M. *ACS Appl. Mater. Interfaces* **2021**, *13*, 4861−4873.

(27) Wang, Z. Q.; Jia, H. Z.; Zhao, H. R.; Zhang, R.; Zhang, C.; Zhu, K. C.; Guo, X. T.; Wang, T. C.; Zhu, L. Y. *Environ. Sci. Technol.* **2022**, *56*, 9806−9815.

(28) Parajuli, S.; Miao, W. J. *Anal. Chem.* **2013**, *85*, 8008−8015.

(29) Zheng, L. Y.; Chi, Y. W.; Shu, Q. Q.; Dong, Y. Q.; Zhang, L.; Chen, G. N. *J. Phys. Chem. C* **2009**, *113*, 20316−20321.

(30) Qin, Y. L.; Wang, Z. Q.; Xu, J. N.; Han, F. J.; Zhao, X.; Han, D. X.; Liu, Y.; Kang, Z. H.; Niu, L. *Anal. Chem.* **2020**, *92*, 15352−15360.

(31) Yang, L.; Jia, Y.; Wu, D.; Zhang, Y.; Ju, H.; Du, Y.; Ma, H.; Wei, Q. *Anal. Chem.* **2019**, *91*, 14066−14073.

(32) Zhao, L.; Song, X. Z.; Ren, X.; Fan, D. W.; Wei, Q.; Wu, D. *Anal. Chem.* **2021**, *93*, 8613−8621.